VERTAISARVIOITU
KOLLEGIALT GRANSKAD
PEER-REVIEWED
www.tsv.fi/tunnus

Finite element model for rectangular hollow section T joints

Marsel Garifullin[1], Sami Pajunen, Kristo Mela and Markku Heinisuo

Summary.   Major developments in hardware and software enable researchers and engineers to apply non-linear finite-element analyses to study the behavior of tubular structures. However, to provide reasonable results, constructed finite element models should be verified and validated with experimental data. This article develops a finite element model for high strength steel rectangular hollow section T joints. The joints are considered under in-plane bending moment and axial brace loading. The paper determines the most suitable finite elements and the number of layers in the thickness direction for the numerical assessment of initial stiffness and modeling the whole action-deformation behavior of joints. Finally, the proposed FE model is validated with the series of experimental tests. The validation shows that the developed model properly captures the local behavior of tubular joints and can efficiently serve as a reliable tool in routine numerical analyses.

Key words: hollow section joint, T joint, finite element analysis, initial stiffness, moment resistance

Introduction

The finite element modeling (FEM) represents a powerful tool for analyzing tubular joints under different loading conditions. For a long time, welded hollow section joints have been modelled by shell finite elements, since shell models are simple for modeling and do not require large computational efforts. The pioneering work was conducted by Puthli [1], who first simulated the ultimate load behaviour of tubular joints. Later shell elements were employed by many researchers [2, 3, 4, 5, 6, 7]. Although shell elements are effective for most joints providing accurate results without considerable computational effort, they present certain difficulties in modelling fillet welds. Some methods for the idealization of welds are presented in [8, 9, 10, 11].

   The increasing computing power of modern computers allows researchers to use solid elements to simulate the behavior of tubular joints [12, 13, 14, 15]. In comparison to shell elements, the main advantage of solid ones is the simple modelling of welds, which allows to repeat exactly the geometry of welds. Some comparative analyses on the use of shell and solid elements have been conducted in [16, 17]. According to [18], the most

---

[1]Corresponding author: marsel.garifullin@tut.fi

accurate results for tubular joints are provided by using solid models. The paper [19] provides a broad discussion concerning the FE analysis of welded hollow-section joints, paying attention to the most actual problems.

However, the broad application of solid elements presents the problem of selecting suitable finite elements. Currently, the following solid elements are available for meshing 3D models: tetrahedra, triangular prisms (wedges) and hexahedra (bricks) [20]. Generally, tubular joints are modelled with bricks. However, even within bricks, the choice of available elements is rather wide: there are linear and quadratic elements, elements with full and reduced integration, elements with incompatible modes and hybrid elements. Each element is developed for particular types of tasks. In most of scientific tasks, the choice of a proper finite element directly affects the accuracy of the solution; an incorrect selection can lead to unreliable results.

Another important issue in modelling is the number of elements in the thickness direction, i.e., the number of layers. Generally, increasing the number of layers improves the accuracy of the analysis. However, this simultaneously increases the number of degrees of freedom in the whole model, being computationally very expensive. For this reason, the correct number of layers is very important to provide an accurate solution within a reasonable calculation time.

According to [19], at least two quadratic solid elements are recommended in the thickness direction to properly model the behavior of tubular joints. However, models with such mesh are computationally very demanding and thus require considerable calculation time. At the same time, some engineering tasks [21, 22] require only initial stiffness of joints, without considering their resistance and whole action-deformation responses. In such tasks, FEM should provide a fast tool for evaluation of joints performance, making calculation time the limiting factor.

This article develops a finite element model for rectangular hollow section (RHS) T joints. A typical RHS T joint is composed of two hollow section members welded at an angle of 90°, as shown in Figure 1. Joints with fillet and butt welds are considered under two loading cases: in-plane bending and axial brace loading, as demonstrated in Figure 2. The paper identifies the most suitable finite element and the number of layers in the thickness direction by the criteria of accuracy of results and reasonable calculation time. The verification is conducted in terms of initial stiffness and the whole load-deformation behavior of joints. Finally, the constructed FE model is validated with

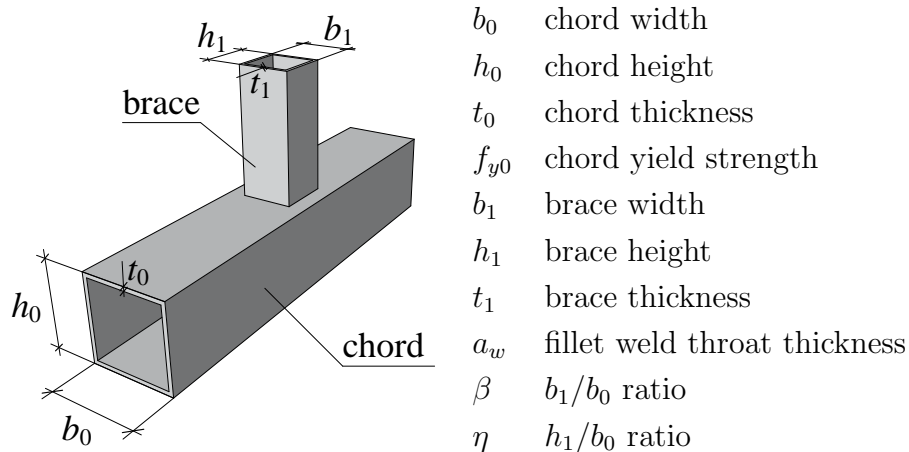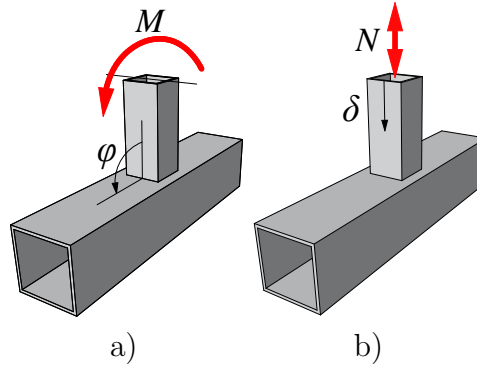|	
b_0	chord width
h_0	chord height
t_0	chord thickness
f_{y0}	chord yield strength
b_1	brace width
h_1	brace height
t_1	brace thickness
a_w	fillet weld throat thickness
β	b_1/b_0 ratio
η	h_1/b_0 ratio

Figure 1. Notations of RHS T joint.

Figure 2. Loading cases: a) in-plane bending; b) axial brace loading.

experimental data available in the literature. All analyses employ a general purpose FE software Abaqus/Standard [20].

Structural behavior of RHS T joints

The behavior of tubular joints demonstrates certain similarities in case of in-plane bending and axial brace loading and can be idealized using local beam models. A local beam model for semi-rigid RHS T joints has been developed in [23] and is presented in Figure 3. The rotational and longitudinal springs represent rotational and axial stiffness for in-plane bending moment and axial brace loading, with initial values $S_{j,ini}$ and $C_{j,ini}$, respectively. Here S corresponds to rotational stiffness and C to axial stiffness. In accordance with EN 1993-1-8:2005 [24], the subscripts j and ini correspond to "joint" and "initial phase", respectively. It should be noted that the springs are located at the upper flange of the chord and connected to the chord axis by a rigid beam [25].

The initial stiffness and resistance of tubular joints can be found from corresponding action-deformation curves, which are obtained from experimental tests or numerical simulations. For convenience, both loading cases are considered simultaneously: the first notation corresponds to in-plane bending, while the one in brackets – to axial loading. In particular, initial stiffness $S_{j,ini}$ ($C_{j,ini}$) is found as the tangent line in the elastic phase of the curve, as shown in Figure 4a:

$$S_{j,ini} = \Delta M / \Delta \varphi$$
$$C_{j,ini} = \Delta N / \Delta \delta \tag{1}$$

The determination of resistance is generally more complicated and depends on the
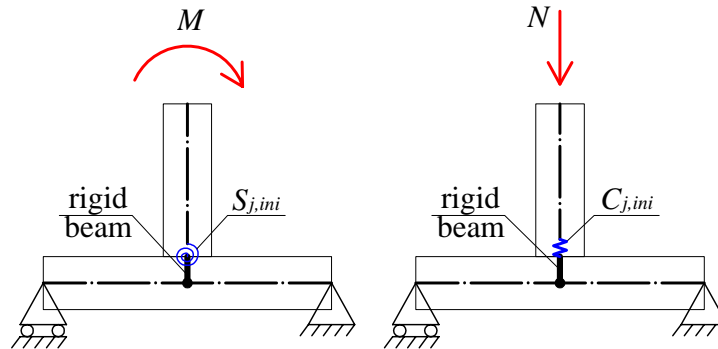

Figure 3. Design local models for RHS T joint under in-plane bending and axial brace loading.
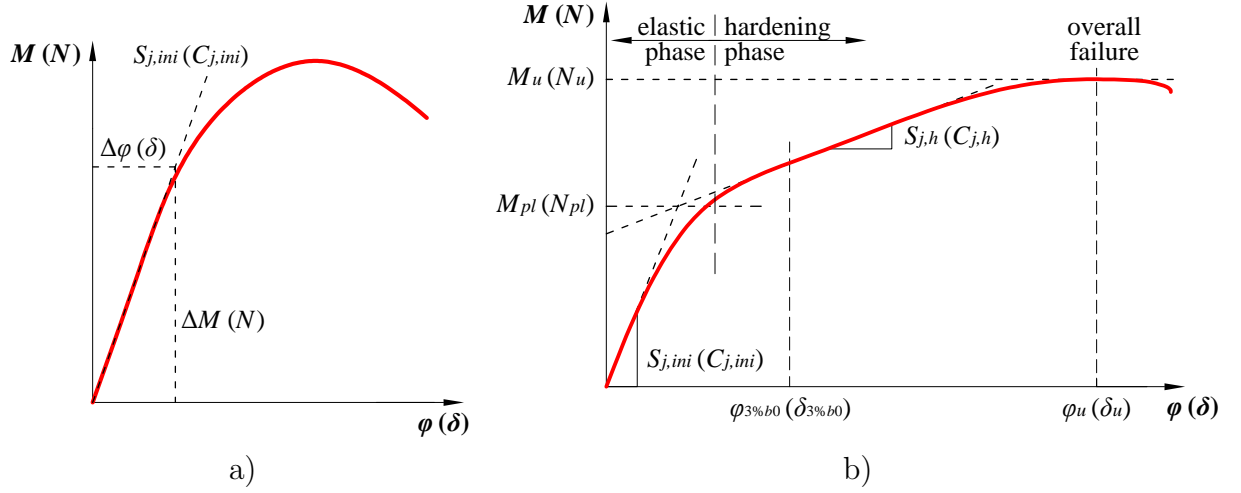
Figure 4. Action-deformation curve for T joints: a) determination of initial stiffness; b) resistance of joints with $\beta \leq 0.85$.

brace-to-chord width ratio β. For joints with $\beta \leq 0.85$, bending of the chord top face governs the deformation of the whole joint, and the action-deformation curve has a clearly observed hardening phase, as depicted in Figure 4b. In this case, plastic resistance M_{pl} (N_{pl}) is determined according to [26] as the intersection of two tangent lines corresponding to initial stiffness $S_{j,ini}$ $(C_{j,ini})$ and hardening stiffness $S_{j,h}$ $(C_{j,h})$. Ultimate resistance M_u (N_u) corresponds to the maximum load the joint can resist. Theoretically, the resistance of such joints is computed according to Tables 7.11 and 7.14 of EN 1993-1-8:2005 [24]:

$$M_{ip,1,Rd} = k_n f_{y0} t_0{}^2 h_1 \left(\frac{1}{2\eta} + \frac{2}{\sqrt{1-\beta}} + \frac{\eta}{1-\beta} \right) / \gamma_{M5}$$

$$N_{1,Rd} = \frac{k_n f_{y0} t_0{}^2}{1-\beta} \left(2\eta + 4\sqrt{1-\beta} \right) / \gamma_{M5} \tag{2}$$

where $\gamma_{M5} = 1.0$ is the partial safety factor, $k_n \leq 1.0$ is the chord stress function, which allows to consider the influence of axial stresses in the chord [24]. The remaining notations are determined in Figure 1.

The behavior of joints with $0.85 < \beta \leq 1.0$ is generally governed by chord side walls buckling [24]. Instead of a well-developed hardening phase, the action-deformation curves of such joints have a clear peak load M_{max} (N_{max}). To evaluate the resistance of the joint, the $3\%b_0$ deformation limit is calculated in accordance with [27]. This limit restricts local deformations of the joint to 3% from the chord width. For a joint loaded by an in-plane bending moment and an axial force, the deformation limits are respectively found as

$$\varphi_{3\%b0} = \frac{0.03 b_0}{h_1/2} = \frac{0.06}{\eta}$$

$$\delta_{3\%b0} = 0.03 b_0 \tag{3}$$

According to [28], the resistance of such joints depends on the correlation between the peak load and the $3\%b_0$ deformation limit. If a joint has a peak load M_{max} (N_{max}) at a deformation smaller than $\varphi_{3\%b0}(\delta_{3\%b0})$, the peak load is considered to be the resistance of the joint, as shown in Figure 5a. If a joint has a peak load M_{max} (N_{max}) at a deformation larger than $\varphi_{3\%b0}(\delta_{3\%b0})$, the resistance is determined as equal to the load at the deformation limit (Figure 5b). Theoretically, the resistance corresponding to chord side walls
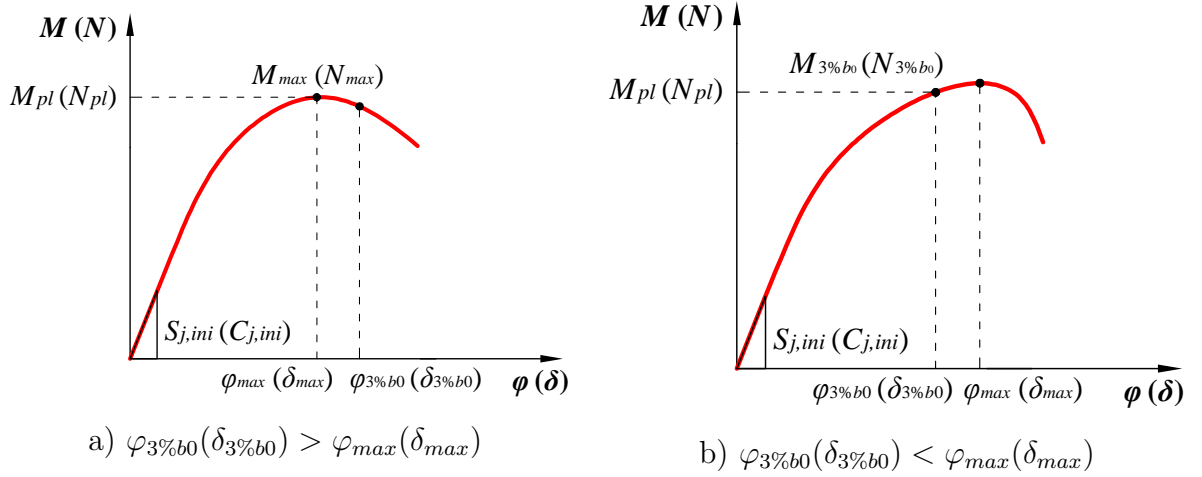
Figure 5. Action-deformation curve for T joints with $0.85 < \beta \leq 1.0$.

buckling is computed in accordance with Tables 7.11 and 7.14 of EN 1993-1-8:2005 [24]:

$$
\begin{aligned}
M_{ip,1,Rd} &= 0.5 f_{y0} t_0 (h_1 + 5t_0)^2 / \gamma_{M5} \\
N_{1,Rd} &= f_b t_0 \left(2h_1 + 10t_0\right) / \gamma_{M5}
\end{aligned}
\tag{4}
$$

where f_b is specified in Table 7.11 of EN 1993-1-8:2005. The remaining notations are determined in Figure 1.

Finite element model for RHS T joints

Development of FE model

All sections are modelled with round corners. To exclude possible effects of chord boundary conditions, the length of the chord is selected to be $6b_0$, as recommended in [29], while the brace length is taken to be $4b_1$. The members are meshed using solid hexahedral elements, being refined near the joint, as depicted in Figure 6a. The recommended mesh size is determined to be $t_0/2$. The proper finite element type and the number of elements in the thickness direction are evaluated in the following sections.
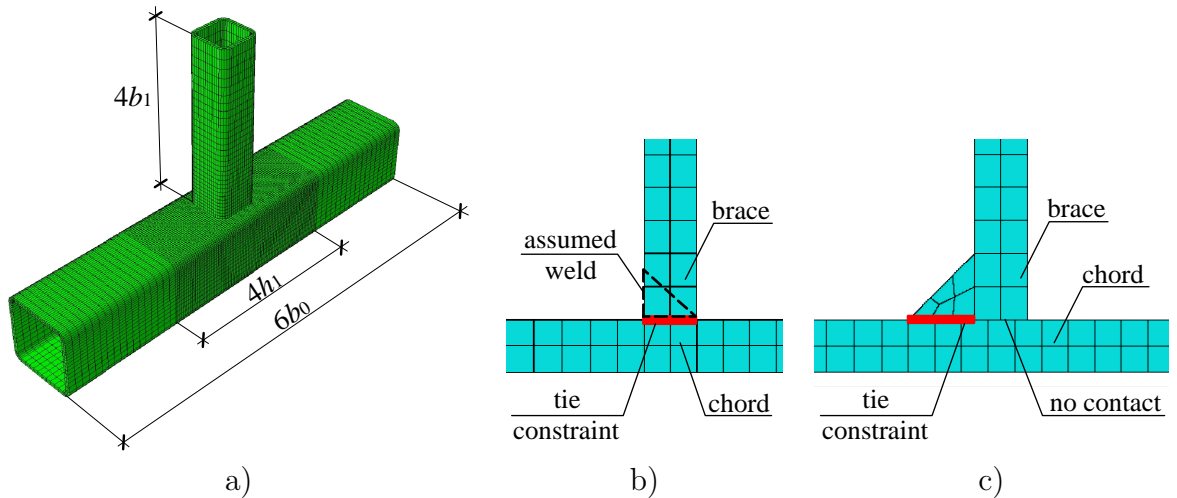

Figure 6. FE model: a) meshing; b) butt welds modeling; c) fillet welds modeling.

In this study, joints with butt and fillet welds are considered. Butt welds are modelled as the base material of the brace, as shown in Figure 6b. The contact between the connected members is modelled using the tie constraint, which ties two surfaces together with no relative motion between them. This tool is used by many researchers [30, 23, 31] and it allows to use independent meshes for the connected members without matching their nodes, thus considerably reducing the labor intensity of the modelling process.

Fillet welds are modelled as a part of the brace, repeating their actual geometry, as shown in Figure 6c. The contact between the weld and the chord is modelled with the tie constraint; however, no interaction is introduced between the brace and the chord. Strictly speaking, the contact between the brace and the chord should be modelled with the contact interaction to avoid possible penetration of brace nodes into the chord resulted from compressive loads. However, it has been shown that the penetration takes place only at very large deformations and does not influence the results in the practical range of interest [32]. It should be noted that for equal-width joints ($\beta = 1.0$), longitudinal fillet welds cannot be performed and are replaced by partial/full penetration butt welds.

Material properties can be modelled with true stress-strain curves obtained from tensile coupon tests, or employing one of the simplified models proposed in Appendix C.6 of EN 1993-1-5:2006 [33]. Loading is brought about by a force-controlled nonlinear static analysis, applying a concentrated in-plane moment M or an axial force N to the reference point connected rigidly with the end of the brace. If the joint is simply supported at its ends, the axial force N causes in-plane bending in the chord, producing additional normal stresses on its faces [34]. These stresses affect the structural behaviour of tubular joints, reducing their resistance and initial stiffness. To consider the behaviour of joints under pure axial load, this effect should be eliminated by several possible approaches. The most reliable one employs a contact interaction with a "rigid floor" modelled with extremely stiff elements, as shown in Figure 7a. Although this method as accurately as possible simulates the real behavior, it is computationally very demanding. The second approach introduces constraints against vertical displacements along the length of the chord, as shown in Figure 7b. This technique is rather simple but it allows no disconnection between the contacted surfaces during the loading process. For this reason, it slightly overestimates the stiffness of the model. The third method applies compensating moments $M_0 = 0.25N(L_0 - h_1)$ at the ends of the chord, resulting in zero bending moment on the area of connection [34], as shown in Figure 7c.
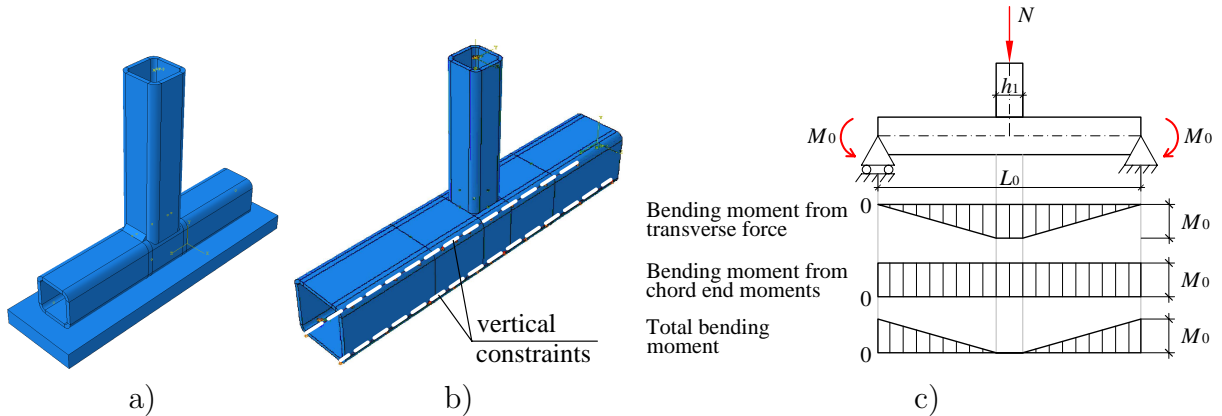

Figure 7. Possibilities to eliminate chord bending: a) contact interaction with "rigid floor"; b) vertical constraints; b) compensating moments.

Extracting local deformations of joints

To construct the action-deformation curve of the joint, applied forces and moments as well as the corresponding displacements and rotations are measured during the loading. Generally, measured displacements and rotations reflect the global behavior of the joint, which includes the deformations of the chord and the brace, as well as the local deformations of the joint. The latter represents the deformations at the connection area, where the brace and the chord meet. To obtain the local rotation of the joint φ in case of in-plane bending, the rotation of the brace φ_{br} and the rotation of the chord φ_{ch} are subtracted from the rotation in the end of the brace φ_{tot} (Figure 8):

$$\varphi = \varphi_{tot} - \varphi_{br} - \varphi_{ch} \tag{5}$$

In case of axial loading, two parameters are measured in FEM: the vertical displacement in the end of the brace δ_{br} and the vertical displacement in the bottom flange of the chord δ_{bot}, as shown in Figure 9. The local displacement of the joint δ is then

$$\delta = \delta_{br} - \delta_{bot} - \delta_{sh} \tag{6}$$

where δ_{sh} is the shortening of the brace. If the bending of the chord is prevented by any of the methods depicted in Figure 7, δ_{bot} can be considered as equal to zero. The motions of the members are supposed to be elastic (assuming that plastic deformations occur only in the connection area); therefore, the values φ_{br}, φ_{ch}, and δ_{sh} are calculated manually using the engineering beam theory:

$$\varphi_{br} = \frac{ML_1}{EI_1}; \varphi_{ch} = \frac{ML_0}{12EI_0}; \delta_{sh} = \frac{NL_1}{EA_1} \tag{7}$$

where L_0 and L_1 are, respectively, the lengths of the chord and the brace, I_0 and I_1 are, respectively, the second moments of area of the chord and the brace, A_1 is the cross-sectional area of the brace, and E is Young's modulus. It should be noted that the motions of the brace, φ_{br} and δ_{sh}, can be eliminated in advance by modelling the brace with the Young's modulus considerably higher than that of the chord. Since the local deformations of the joint are represented by the deformations of the chord, this approach causes no losses of accuracy in the analysis.
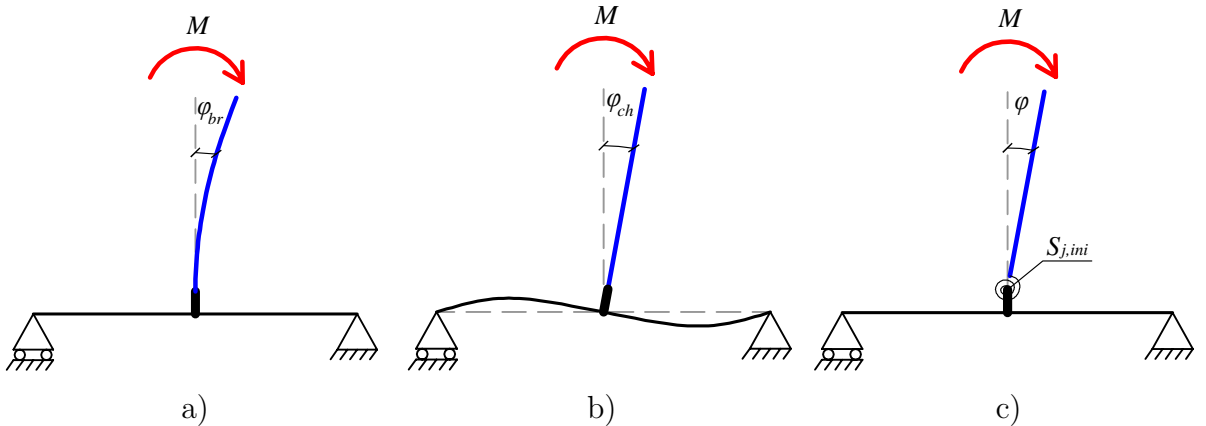

Figure 8. Behavior of the T joint under bending moment: a) elastic rotation of the brace; b) elastic rotation of the chord; c) local rotation of the joint.
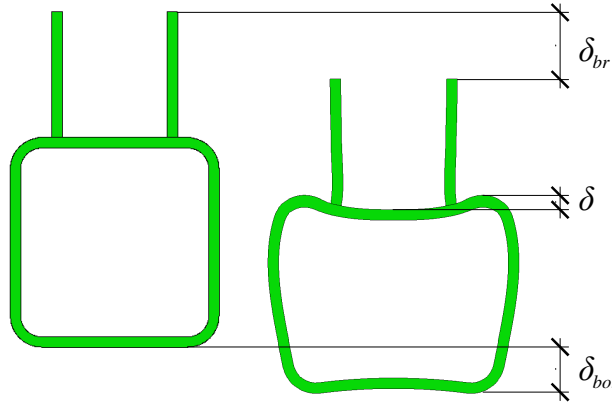
Figure 9. Definition of local behavior under axial loading.

Initial imperfections

To provide reliable results, a FE model must also incorporate initial imperfections that are obviously always present in real structures. In relation to tubular joints, initial imperfections include geometrical imperfections, welding residual stresses and residual stresses due to cold-forming. However, it was shown that the negative influence of geometrical imperfections on the behavior of tubular joints is inconsiderable, generally accounting for 1-2% [35]. In addition, the comparative parametric analysis demonstrated that the consideration of welding stresses in the FE analysis leads to greater resistance of tubular joints [36]. The influence of residual stresses due to cold-forming was found also insignificant [37]. For this reason, tubular joints can be considered as not sensitive to initial imperfections and can be safely modelled with no imperfections.

Search of best finite element and number of elements in the thickness direction for initial rotational stiffness

This section determines the most suitable finite element and the number of elements in the thickness direction that are required to accurately determine the initial rotational stiffness of the RHS T joint under in-plane bending. All analyses are conducted for a square hollow section T joint with a 200x200x8.8 mm chord and three braces: 50x50x4 mm ($\beta = 0.25$), 100x100x8 mm ($\beta = 0.50$) and 150x150x8.8 mm ($\beta = 0.75$). For simplicity, the section considers only joints with butt welds. Since only initial stiffness is analyzed in this section, the load is applied using a single increment. Assuming that initial stiffness is calculated in the elastic phase of the loading process, only elastic properties are introduced to the material model, with the Young's modulus of 210 GPa and the Poisson's ratio of 0.3. The study analyzes five types of finite elements available in Abaqus for static analyses: C3D8, C3D8R, C3D8I, C3D20 and C3D20R. The details of the elements are provided in Table 1. To investigate the number of elements in the thickness direction, the joints are modelled with one-, two-, three- and four-layered mesh.

Figure 10 presents the initial stiffness of the analyzed joints depending on the element type and the number of layers. As can be seen, linear reduced integrated elements (C3D8R) considerably underestimate the stiffness of the joints, leading to zero stiffness for the one-layered mesh. Such behavior can be explained by the hourglass effect, which is typical for linear reduced-integration elements [38]. To avoid this effect, the Abaqus manual [20] suggests at least four C3D8R elements in the thickness direction for any

22

Table 1. Analyzed finite elements [20]

Finite element	Type	Number of nodes	Remarks
C3D8	linear	8	full integration
C3D8R	linear	8	reduced integration
C3D8I	linear	8	incompatible modes
C3D20	quadratic	20	full integration
C3D20R	quadratic	20	reduced integration

structures under bending loads. However, the obtained results demonstrate that even four C3D8R elements are insufficient for tubular joints, underestimating the stiffness by 10-11%. Fully integrated linear elements (C3D8) similarly underestimate the stiffness, although the error is not as large as for C3D8R elements. The error declines with mesh refinement and can be neglected using at least three elements in the thickness direction.

The most relevant results are obtained using quadratic finite elements (C3D20 and C3D20R). In both cases, the stiffness declines asymptotically with mesh refinement. Moreover, both elements perform similarly, providing reliable results even with a one-layered mesh. At the same time, reduced integrated elements (C3D20R) require noticeably less calculation time than fully integrated elements (C3D20). These observations correspond to [19], who propose at least two quadratic solid elements in the thickness direction.

Attention should be paid particularly to linear elements with incompatible modes (C3D8I), designed to overcome the problems of shear locking [39]. Compared to quadratic finite elements, C3D8I elements need considerably less calculation time, providing very accurate results if not distorted [39]. In this study, these elements show initial stiffness very close to that calculated by quadratic finite elements, being not dependent on the number of elements in the thickness direction. From this point of view, C3D8I elements can be suggested for quick evaluations of initial stiffness, e.g. in surrogate modeling [22].

Based on the above findings, quadratic finite elements (C3D20 or C3D20R in Abaqus) are recommended to calculate the initial stiffness of RHS T joints. Reduced integration elements (C3D20R) are more preferable, since they require less computational time. Linear elements with incompatible modes (C3D8I in Abaqus) can also be used for this purpose. At least two elements in the thickness direction are sufficient. If calculation time is important, a one-layered mesh can also be utilized, leading to slight losses in accuracy. It should be noted that these findings are obtained for the joints with $\beta \leq 0.85$, i.e., when chord
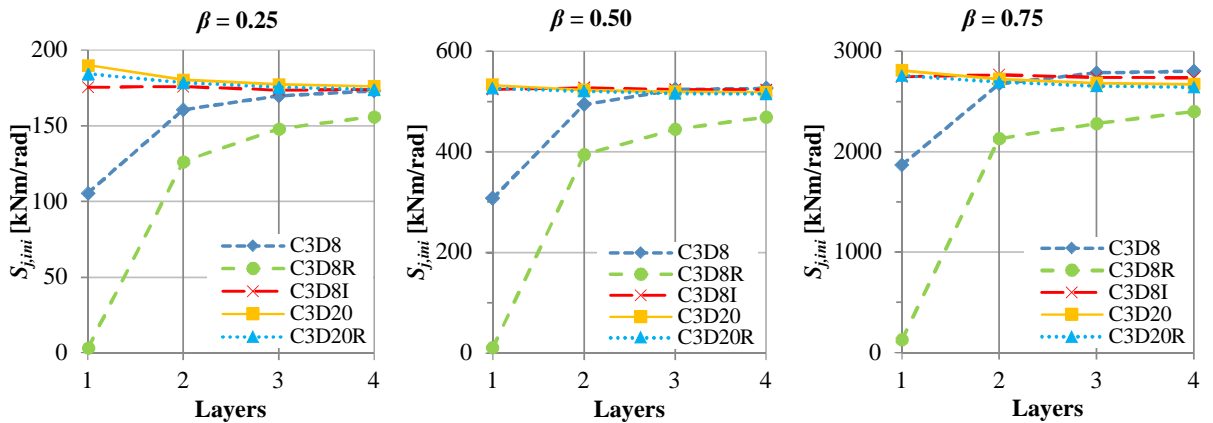

Figure 10. Initial rotational stiffness as function of finite element type and number of layers.

face bending governs the behaviour of the joint. According to EN 1993-1-8:2005 [24], this failure mode is also critical for other loading cases when $\beta \leq 0.85$, including axial loading and out-of-plane bending. Therefore, the obtained conclusions can be justified also for these loading cases.

Search of best finite element and number of elements in the thickness direction for moment resistance

The previous section has shown that at least two C3D8I or C3D20R elements in the thickness direction has to be used to calculate the initial stiffness of tubular joints. This section determines the most suitable finite element and the required number of layers considering the whole loading process until the failure of the joint. The study analyses the joints employed in the previous section. Only C3D8I and C3D20R finite elements are applied with one-, two- and three-layered mesh. The joints are evaluated by the ultimate moment resistance, determined as the maximum moment the joint can resist. Every analysis is conducted considering geometrical and material nonlinearity, employing the elastic-perfectly plastic material model in accordance with Appendix C.6 of EN 1993-1-5:2006 [33]. All analyses are performed by measuring calculation time on a personal computer with an Intel Core i7-2600 CPU with 3.40 GHz clock frequency and a 16 GB RAM, using multiple processors parallelization. Following the conclusions of the previous section, the models with three quadratic C3D20R elements in the thickness direction are deduced to provide the most exact moment resistance ($M_{u,20,3}$), and other models are compared to them.

Table 2 presents absolute (M_u) and relative ($M_u/M_{u,20,3}$) moment resistances as well as the calculation time obtained from FEM. As expected, the most reliable results are obtained by using quadratic finite elements (C3D20R), decreasing asymptotically with the increase of the number of elements in the thickness direction. The models with one C3D20R element in the thickness direction overestimate resistance by 5%, while the ones with two C3D20R elements provide almost the same values. The calculation time is crucial, accounting for at least 5 hours for the three-layered mesh models. From that point of view, two C3D20R elements in the thickness direction provide the most preferable solution by the criteria of accuracy and calculation time. Three elements in the thickness direction bring no reasonable improvement of accuracy, increasing the calculation time more than two times. These conclusions are in line with the recommendations of [19].

Linear finite elements with incompatible nodes (C3D8I) also provide accurate results. However, the maximum error of 10% makes them unreliable for numerical simulations,

Table 2. Moment resistance verification

Element type	Number of elements	$\beta = 0.25$			$\beta = 0.50$			$\beta = 0.75$		
		M_u [kNm]	$\dfrac{M_u}{M_{u,20,3}}$	t [min]	M_u [kNm]	$\dfrac{M_u}{M_{u,20,3}}$	t [min]	M_u [kNm]	$\dfrac{M_u}{M_{u,20,3}}$	t [min]
C3D8I	1	6.60	1.00	8	40.17	1.09	11	83.86	1.05	13
	2	6.61	1.00	20	40.60	1.10	28	81.69	1.02	29
	3	6.61	1.00	29	40.18	1.09	36	81.95	1.02	55
C3D20R	1	6.63	1.00	38	38.60	1.05	61	83.25	1.04	56
	2	6.62	1.00	135	37.19	1.01	122	80.00	1.00	181
	3	6.62	1	323	36.75	1	283	80.13	1	400

even when using three elements in the thickness direction. At the same time, the main advantage of C3D8I elements is low calculation time: even three C3D8I elements in the thickness direction are less time-consuming than one C3D20R element. From that point of view, C3D8I elements can be suggested for quick FE analyses without strict requirements of accuracy.

Validation of developed FE model

To ensure that the developed FE model can be efficiently employed to predict the structural behaviour of RHS joints, it is validated with experimental data available in the literature. The model is constructed following the above findings, with two quadratic solid elements in the thickness direction, both for the brace and the chord. The validation evaluates the initial stiffness and resistance of joints under in-plane bending moment and axial brace loading. As initial imperfections are found to have no influence on the behavior of tubular joints, they are neglected in the validation. For comparison, the resistance is also calculated theoretically according to EN 1993-1-8:2005 [24]. In the following figures, $M_{pl,exp}$ ($N_{pl,exp}$), $M_{pl,FEM}$ ($N_{pl,FEM}$) and $M_{pl,theory}$ ($N_{pl,theory}$) denote, respectively, plastic bending (axial) resistance determined experimentally, numerically and theoretically.

HAMK tests

The first validation is conducted with the tests of Häme University of Applied Sciences (HAMK) [40]. The experiments on square hollow section T joints under in-plane bending moment were performed by varying section dimensions, steel grades and weld sizes. Three types of welds were analyzed: 6 mm fillet welds, 10 mm fillet welds and 1/2v butt welds. The details of the joints are presented in Table 3, where the naming of the test specimens is presented in the format [chord steel grade]_[brace steel grade]_[weld type]. The joints are modelled with the measured section dimensions of the specimens. The actual throat thicknesses of welds were not measured; therefore, the study employs nominal values. The material properties were obtained from tensile coupon tests.

Figure 11a shows the comparison between the deformation patterns obtained experimentally and numerically for case S420_S420_a6. As can be seen in the figure, the model efficiently captures the chord face failure and the buckling of chord side walls. The moment-rotation curves for this case are presented in Figure 11b, and the remaining cases are considered in Appendix 1. Good agreement is observed between the results in the elastic phase, with a slight discrepancy in the hardening phase. The most exact prediction is observed for the joints with 6 mm welds, almost repeating the experimental moment-rotation curves. The cases with 10 mm welds have the largest visual difference between the experimental and numerical results in the hardening zone, which can be probably caused by the difference in the material properties.

The summary of the results is presented in Table 4. As can be seen, the prediction of the initial rotational stiffness is rather accurate almost for all joints. The largest errors are observed for cases S500_S500_a6 and S500_S500_a10, which can be caused by unexpectedly low experimental stiffness in comparison to the corresponding cases with the same geometry. Bending resistance is predicted accurately, being slightly underestimated for the joints with 10 mm fillet and butt welds. The largest discrepancy is observed for the cases with the large braces, i.e., S700_S700_a6 and S700_S700_a10. The experimental and numerical results correlate well with the theoretical values, particularly for the joints with butt welds. At the same time, the observed error increases with the rise of the weld

Table 3. HAMK tests: details of joints

Joint	b_0 [mm]	h_0 [mm]	t_0 [mm]	b_1 [mm]	h_1 [mm]	t_1 [mm]	β	a_w [mm]	E [GPa]	f_{y0} [MPa]
S420_S420_a6				100	100	8	0.67		185	507
S500_S420_a6				100	100	8	0.67		196	602
S500_S500_a6				100	100	8	0.67		196	602
S700_S420_a6	150	150	8	100	100	8	0.67	6	197	769
S700_S500_a6				100	100	8	0.67		197	769
S700_S700_a6				120	120	8	0.80		197	769
S420_S420_a10				100	100	8	0.67		185	507
S500_S420_a10				100	100	8	0.67		196	602
S500_S500_a10				100	100	8	0.67		196	602
S700_S420_a10	150	150	8	100	100	8	0.67	10	197	769
S700_S500_a10				100	100	8	0.67		197	769
S700_S700_a10				120	120	8	0.80		197	769
S420_S420_1/2v				100	100	8	0.67		185	507
S500_S420_1/2v				100	100	8	0.67		196	602
S500_S500_1/2v				100	100	8	0.67		196	602
S700_S420_1/2v	150	150	8	100	100	8	0.67	butt	197	769
S700_S500_1/2v				100	100	8	0.67		197	769
S700_S700_1/2v				120	120	8	0.80		197	769

size, leading to a significant overestimation of resistance for 10 mm welds. This fact can be explained by the improving effect of fillet welds: welds enlarge the cross-section of the brace in the contact area, increasing thus the total length of the yield mechanism and the resistance of the joint [41]. Currently, this effect is not considered in EN 1993-1-8:2005, leading to a very conservative theoretical resistance for the joints with large fillet welds.
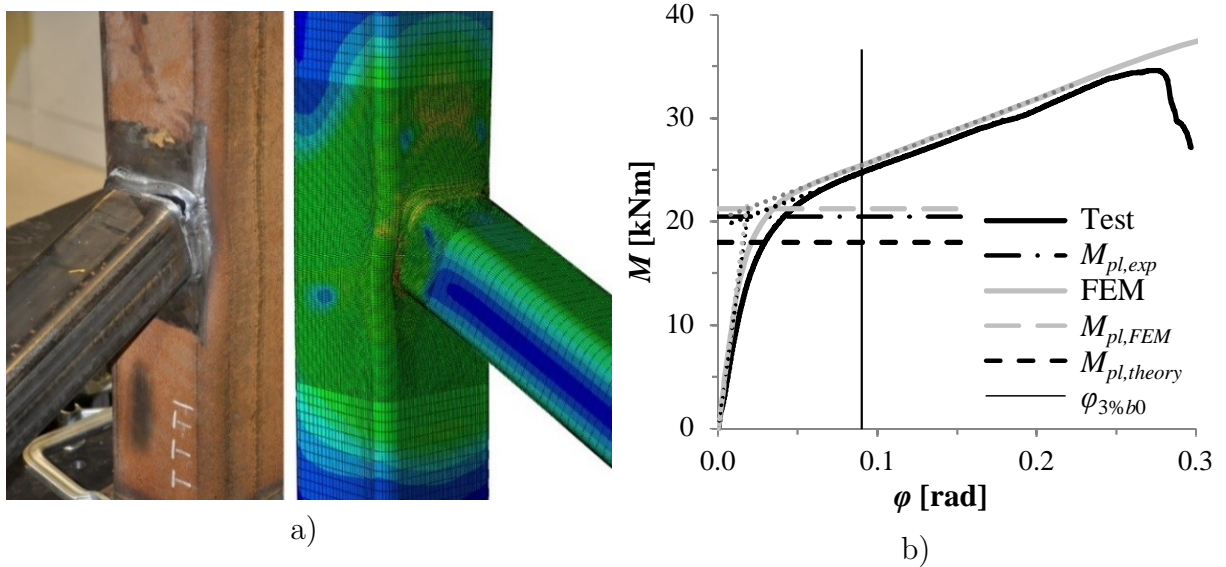

Figure 11. S420_S420_a6: a) correlation between test and FEM; b) moment-rotation curves.

Table 4. HAMK tests: validation

Joint	$S_{j,ini}$ [kNm/rad]			M_{pl} [kNm]				
	FEM	Test	FEM / Test	FEM	Test	Theory	FEM / Test	FEM / Theory
S420_S420_a6	1189	1115	1.07	21.2	20.5	18.0	1.04	1.18
S500_S420_a6	1231	1083	1.14	24.3	23.6	19.3	1.03	1.26
S500_S500_a6	1277	995	1.28	25.1	24.7	19.3	1.02	1.30
S700_S420_a6	1231	1082	1.14	28.4	27.1	24.1	1.05	1.18
S700_S500_a6	1257	1108	1.13	29.4	28.9	24.1	1.02	1.22
S700_S700_a6	2178	1990	1.09	43.0	59.0	42.1	0.73	1.02
Average			1.14				0.98	1.19
S420_S420_a10	1681	1692	0.99	29.4	31.8	18.1	0.92	1.63
S500_S420_a10	1762	1701	1.04	33.2	34.9	19.3	0.95	1.72
S500_S500_a10	1837	1452	1.26	35.2	37.3	19.3	0.94	1.82
S700_S420_a10	1603	1521	1.05	36.3	38.5	23.9	0.94	1.52
S700_S500_a10	1736	1705	1.02	39.3	45.7	24.0	0.86	1.64
S700_S700_a10	2242	2268	0.99	44.1	64.0	42.5	0.69	1.04
Average			1.06				0.88	1.56
S420_S420_1/2v	888	893	0.99	15.7	18.2	18.2	0.86	0.86
S500_S420_1/2v	963	977	0.99	18.7	20.9	19.3	0.89	0.97
S500_S500_1/2v	941	1003	0.94	18.6	20.4	19.3	0.91	0.96
S700_S420_1/2v	940	971	0.97	22.5	23.4	24.0	0.96	0.94
S700_S500_1/2v	967	961	1.01	23.0	25.6	24.3	0.90	0.94
S700_S700_1/2v	2091	1990	1.05	43.6	44.7	43.7	0.98	1.00
Average			0.99				0.91	0.94

Tests of TH Karlsruhe and Kobe University

This validation is performed using tests M44 and M45 conducted in the TH Karlsruhe [17] and tests S12, S23, R2, R4 conducted in the Kobe University [42]. All specimens were made of cold-formed sections. The moment-rotation curves of the joints are presented in [26]. The details of the joints are provided in Table 5. The simulation employs a bi-linear elasto-plastic material model with strain hardening based on the provided yield and ultimate stresses with the corresponding elongations.

The experimental and numerical curves are presented in Appendix 2, the comparison

Table 5. Tests of TH Karlsruhe and Kobe University: details of joints

Joint	b_0 [mm]	h_0 [mm]	t_0 [mm]	b_1 [mm]	h_1 [mm]	t_1 [mm]	β	a_w [mm]	E [GPa]	f_{y0} [MPa]
M44	160	160	4	100	100	3	0.63	3	210	420
M45	160	160	5	100	100	3	0.63	3	210	420
S12	200	200	9	150	150	6	0.75	6	210	235
S23	250	250	6	175	175	6	0.70	6	210	235
R2	200	200	6	100	200	6	0.50	6	210	235
R4	200	200	6	152	254	6.4	0.76	6	210	235

Table 6. Tests of TH Karlsruhe and Kobe University: validation

Joint	$S_{j,ini}$ [kNm/rad]			M_{pl} [kNm]				
	FEM	Test	FEM / Test	FEM	Test	Theory	FEM / Test	FEM / Theory
M44	146	130	1.12	2.2	2.6	2.2	0.87	1.04
M45	260	260	1.00	3.7	4.8	3.4	0.78	1.11
S12	2745	2000	1.37	31.2	36.4	21.9	0.86	1.43
S23	953	875	1.09	11.1	13.0	9.9	0.85	1.12
R2	702	625	1.12	10.3	9.4	9.0	1.09	1.14
R4	4626	4000	1.16	31.0	34.3	21.0	0.90	1.48
Average			1.14				0.89	1.22

of the results is provided in Table 6. The numerical simulations are found to slightly overestimate the initial stiffness of the joints, which can probably be caused by the nominal dimensions of the sections used in the FE analyses. Experimental plastic resistance is underestimated by 15-20%, except the case R2. This can be explained by the simplified bi-linear material model used in the simulation. Compared to theoretical results, all numerical models demonstrate safe resistance.

Tests of Nizer et al.

The next validation is performed against the tests of Nizer et al. [6]. The tests represent RHS T joints simultaneously loaded by axial forces in the brace and the chord. All specimens were made of ASTM-A36 steel, had the same geometry but differed by the value of the axial force N_0 applied in the chord, as shown in Table 7. Joints TN01N0 and TN02N0 differed by the boundary conditions of the chord: the chord ends were free to rotate for joint TN01N0 but restricted for joint TN02N0. The FE analyses employ a bi-linear elasto-plastic material model with strain hardening based on the provided yield and ultimate stresses with the corresponding elongations.

Following the experiments, the axial force in the chord N_0 is applied in the FE model prior to the static brace loading. It should be noted that in the experiments and the corresponding numerical simulations, the specimens are not vertically supported along the length of the chord, in contrast to Figure 7. This enables the in-plane bending of the chord, producing normal stresses on its upper flange. For this reason, theoretical resistance is calculated considering a chord stress function according to [34].

Table 7. Tests of Nizer et al.: details of joints

Joint	b_0 [mm]	h_0 [mm]	t_0 [mm]	b_1 [mm]	h_1 [mm]	t_1 [mm]	β	a_w [mm]	E [GPa]	f_{y0} [MPa]	N_0 [kN]
TN01N0	140	80	4	100	100	3	0.71	5	200	361.9	0
TN02N0	140	80	4	100	100	3	0.71	5	200	361.9	0
TN03N50+	140	80	4	100	100	3	0.71	5	200	361.9	306.9
TN04N70+	140	80	4	100	100	3	0.71	5	200	361.9	429.6
TN06N50-	140	80	4	100	100	3	0.71	5	200	361.9	-306.9
TN05N70-	140	80	4	100	100	3	0.71	5	200	361.9	-429.6

Table 8. Tests of Nizer et al.: validation.

Joint	$C_{j,ini}$ [kN/mm]			N_{pl} [kN]				
	FEM	Test	FEM / Test	FEM	Test	Theory	FEM / Test	FEM / Theory
TN01N0	140	155	0.90	84.4	84.5	65.5	1.00	1.29
TN02N0	140	280	0.50	84.4	90.1	65.5	0.94	1.29
TN03N50+	143	280	0.51	93.6	97.9	72.3	0.96	1.29
TN04N70+	143	350	0.41	84.0	84.1	72.3	1.00	1.16
TN06N50-	139	140	0.99	73.0	68.6	51.1	1.06	1.43
TN05N70-	137	460	0.30	52.6	52.9	45.3	0.99	1.16
Average			0.60				0.99	1.27

The procedure to calculate plastic resistance described in Figure 4b is applied only for joints TN03N50+ and TN04N70+. The remaining joints demonstrate no clearly observed hardening phase in their load-displacement curves; therefore, their resistance is found as equal to the maximum accepted load. The comparison between the experimental and numerical results is provided in Appendix 3 and summarized in Table 8. The FE model demonstrates good correlation with the experimental results in terms of resistance. Compared to theoretical resistance, the numerical values are safe, providing a sufficient safety margin. At the same time, initial stiffness is noticeably underestimated. This shows that the developed FE model is less sensitive to chord loading: while experimental stiffness is significantly affected by axial loading, numerical model provides almost the same values regardless the applied chord loading.

Tests of Zhao & Hancock

The final validation is performed by using the results of Zhao & Hancock [43]. The paper provides the experimental results of RHS T joints under pure axial load as well as combined axial force and bending moment. Load-displacement curves under pure axial load are provided only for three joints, which details are presented in Table 9. The theoretical resistance of the joints is provided in [28], as well as the improved chord yield stress for joint S1B1C12.

The simulation employs a bi-linear elasto-plastic material model with strain hardening based on the provided yield and ultimate stress with corresponding elongations. During the loading, the joints were located at the stiff floor, eliminating chord bending. Similarly, the numerical simulations employ a contact interaction with a "rigid floor", shown in Figure 7a. The comparison between the experimental and numerical results is illustrated in Appendix 4 and summarized in Table 10. As can be seen, the developed FE model accurately predicts the structural behaviour of the joints, both in relation to initial

Table 9. Tests of Zhao & Hancock: details of joints

Joint	b_0 [mm]	h_0 [mm]	t_0 [mm]	b_1 [mm]	h_1 [mm]	t_1 [mm]	β	a_w [mm]	E [GPa]	f_{y0} [MPa]
S1B1C11	51	102	4.9	51	51	4.9	1.0	4.6	200	379
S1B1C12	51	102	3.2	51	51	4.9	1.0	4.6	200	373
S1B1C23	102	102	4.0	51	51	4.9	0.5	4.6	200	417

Table 10. Tests of Zhao & Hancock: validation

Joint	$C_{j,ini}$ [kN/mm]			N_{pl} [kN]				
	FEM	Test	FEM / Test	FEM	Test	Theory	FEM / Test	FEM / Theory
S1B1C11	619	667	0.93	291.4	307.0	198.0	0.95	1.47
S1B1C12	356	333	1.07	154.9	163.0	80.0	0.95	1.94
S1B1C23	69	50	1.38	60.7	65.6	50.6	0.92	1.20
Average			1.13				0.94	1.54

stiffness and axial resistance. Compared to the theoretical results, the numerical values provide sufficiently safe resistance.

Conclusions

This paper develops a finite element model to analyze welded RHS T joints. The recommendations are provided in relation to the suitable lengths of the connected members, meshing, the modelling of welds and material properties. The paper describes the detailed procedure for extracting the local deformations of the joint from the results of FE analyses. In addition, the study proposes three approaches to eliminate bending of the chord resulted from axial loading.

Attention has been paid particularly on the selection of the suitable finite element and the number of elements in the thickness direction. The conducted analyses show that the choice depends on the requested outcome of the analysis. For initial stiffness, two quadratic solid finite elements with reduced integration in the thickness direction are sufficient. Linear solid elements with incompatible modes can also be used for that purpose, provided that a regular mesh is used. Due to comparatively short calculation time, linear solid elements can present a very efficient tool in engineering tasks based on the extensive computations of the initial stiffness of joints.

At the same time, when the behavior of the joint is considered on the whole phase of loading until its failure, linear solid elements demonstrate errors that cannot be neglected. For this purpose, quadratic elements with reduced integration are the most desirable with at least two elements in the thickness direction. Application of three-layered mesh brings no reasonable improvements in results but severely enlarges calculation time.

The constructed FE model has been validated with the series of experimental tests under in-plane bending moment and axial brace loading. The conducted validation shows that the developed FE model accurately predicts the initial stiffness and resistance of joints. Compared to the theoretical approach based on the current Eurocode, numerical resistance is sufficiently safe. The conducted validation justifies the applicability of the model for further investigations, including extensive parametric studies.

References

[1] Puthli, R. S. Geometrical non-linearity in collapse analysis of thick shells, with application to tubular joints. *Heron* **26** (1981).

[2] Yu, Y. *The static strength of uniplanar and multiplanar connections in rectangular hollow sections* (Delft University of Technology, Doctoral thesis. Delft, 1997).

[3] Al Ali, M., Tomko, M., Demjan, I. & Kvočák, V. Thin-Walled Cold-Formed Compressed Steel Members and the Problem of Initial Imperfections. *Procedia Engineering* **40**, 8–13 (2012). URL https://doi.org/10.1016/j.proeng.2012.07.047.

[4] de Matos, R., Costa-Neves, L., de Lima, L. R., Vellasco, P. & da Silva, J. G. S. Resistance and elastic stiffness of RHS "T" joints: Part I – Axial brace loading. *Latin American Journal of Solids and Structures* **12**, 2159–2179 (2015). URL http://doi.org/10.1590/1679-78251790.

[5] Sarada, S., Fleischer, O. & Puthli, R. Initial Study on the Static Strength of Thin-walled Rectangular Hollow Section (RHS) K-Joints with Gap. *Proceedings of The Twelfth (2002) International Offshore and Polar Engineering Conference, Kitakyushu, Japan, May 26-31, 2002* (2002).

[6] Nizer, A. *et al.* Experimental and numerical assessment of RHS T-joints subjected to brace and chord axial forces. *Steel Construction* **9**, 315–322 (2016). URL https://doi.org/10.1002/stco.201610036.

[7] Tusnina, O. A. & Danilov, A. A. I. The stiffness of rigid joints of beam with hollow section column. *Magazine of Civil Engineering* **4**, 40–51 (2016). URL https://doi.org/10.5862/MCE.64.4.

[8] Christitsas, A., Pachoumis, D., Kalfas, C. & Galoussis, E. FEM analysis of conventional and square bird-beak SHS joint subject to in-plane bending moment – experimental study. *Journal of Constructional Steel Research* **63**, 1361–1372 (2007). URL https://doi.org/10.1016/j.jcsr.2006.12.006.

[9] Lee, M. M. K. Stength, stress and fracture analyses of offshore tubular joints using finite elements. *Journal of Constructional Steel Research* **51**, 265–286 (1999). URL https://doi.org/10.1016/S0143-974X(99)00025-5.

[10] Mang, F., Herion, S. & Bucak, O. Parametric Study on Multiplanar K-Joints with Gap Made of Rectangular Hollow Sections by Means of the Finite Element Method. In *Proceedings of The Third International Offshore and Polar Engineering Conference, Singapore, 6-11 June 1993*, vol. IV, 8–15 (1993).

[11] van der Vegte, G. *The static strength of uniplanar and multiplanar tubular T- and X- joints* (Delft University Press, Doctoral Thesis. Delft, 1995).

[12] Heinisuo, M., Garifullin, M., Jokinen, T., Tiainen, T. & Mela, K. Surrogate modeling for rotational stiffness of welded tubular Y-joints. In Carter, C. J. & Hajjar, J. F. (eds.) *Connections in Steel Structures VIII*, 285–294 (American Institute of Steel Construction, Chicago, Illinois, 2016).

[13] Kosteski, N., Packer, J. A. & Puthli, R. S. A finite element method based yield load determination procedure for hollow structural section connections. *Journal of Constructional Steel Research* **59**, 453–471 (2003). URL https://doi.org/10.1016/S0143-974X(02)00066-4.

[14] Moazed, R., Szyszkowski, W. & Fotouhi, R. The in-plane behaviour and FE modeling of a T-joint connection of thin-walled square tubes. *Thin-Walled Structures* **47**, 816–825 (2009). URL https://doi.org/10.1016/j.tws.2009.01.006.

[15] Shao, Y.-B., Lie, S.-T., Chiew, S.-P. & Huang, Z.-W. Evaluation of geometrical effect on stress distribution for tubular T-joints under axial load. *International Journal of Space Structures* **21**, 77–91 (2006). URL https://doi.org/10.1260/026635106778494372.

[16] Karamanos, S. A., Romeijn, A. & Wardenier, J. Stress concentrations in tubular gap K-joints: mechanics and fatigue design. *Engineering Structures* **22**, 4–14 (2000). URL https://doi.org/10.1016/S0141-0296(98)00062-5.

[17] Mang, F. & Bucak, Ö. *Hohlprofilkonstruktionen. Stahlbauhandbuch* (Stahlbau-Verlag-GmbH, Köln, 1982).

[18] Herion, S., Mang, F. & Puthli, R. Parametric Study on Multiplanar K-Joints with Gap Made of Circular Hollow Sections by Means of the Finite Element Method. In *The Sixth International Offshore and Polar Engineering Conference, Los Angeles, USA May 26-31, 1996*, vol. IV, 68–73 (1996).

[19] van der Vegte, G., Wardenier, J. & Puthli, R. S. FE analysis for welded hollow-section joints and bolted joints. *Proceedings of the Institution of Civil Engineers – Structures and Buildings* **163**, 427–437 (2010). URL https://doi.org/10.1680/stbu.2010.163.6.427.

[20] Abaqus. *Abaqus 6.12. Getting Started with Abaqus: Interactive Edition* (Dassault Systèmes, 695 p., 2012).

[21] Bel Hadj Ali, N., Sellami, M., Cutting-Decelle, A.-F. & Mangin, J.-C. Multi-stage production cost optimization of semi-rigid steel frames using genetic algorithms. *Engineering Structures* **31**, 2766–2778 (2009). URL https://doi.org/10.1016/j.engstruct.2009.07.004.

[22] Garifullin, M. *et al.* Surrogate modeling for initial rotational stiffness of welded tubular joints. *Magazine of Civil Engineering* **3**, 53–76 (2016). URL https://doi.org/10.5862/MCE.63.4.

[23] Haakana, Ä. *In-plane buckling and semi-rigid joints of tubular high strength steel trusses* (Tampere University of Technology, Master of Science Thesis. Tampere, 2014). URL http://URN.fi/URN:NBN:fi:tty-201408281416.

[24] CEN. *Eurocode 3: Design of steel structures – Part 1-8: Design of joints (EN 1993-1-8:2005)* (Brussels, 2005).

[25] Garifullin, M., Pajunen, S., Mela, K. & Heinisuo, M. 3D component method for welded tubular T joints. In Heidarpour, A. & Zhao, X.-L. (eds.) *Tubular Structures XVI: Proceedings of the 16th International Symposium for Tubular Structures (ISTS 2017, 4-6 December 2017, Melbourne, Australia)*, 165–173 (Taylor & Francis Group, London, 2018).

[26] Grotmann, D. & Sedlacek, G. *Rotational stiffness of welded RHS beam-to-column joints. Cidect 5BB-8/98* (RWTH-Aachen, Aachen, 1998).

[27] Lu, L. H., de Winkel, G. D., Yu, Y. & Wardenier, J. Deformation limit for the ultimate strength of hollow section joints. In Grundy, P., Holgate, A. & Wong, B. (eds.) *Tubular Structures VI, 6th International Symposium on Tubular Structures, Melbourne, Australia*, 341–347 (Balkema, Rotterdam, 1994).

[28] Zhao, X.-L. Deformation limit and ultimate strength of welded T-joints in cold-formed RHS sections. *Journal of Constructional Steel Research* **53**, 149–165 (2000). URL https://doi.org/10.1016/S0143-974X(99)00063-2.

[29] van der Vegte, G. & Makino, Y. Further research on chord length and boundary conditions of CHS T- and X-joints. *Advanced Steel Construction* **6**, 879–890 (2010).

[30] AlHendi, H. & Celikag, M. Behavior of reverse-channel and double-reverse-channel connections to tubular columns with HSS. *Journal of Constructional Steel Research* **112**, 271–281 (2015). URL https://doi.org/10.1016/j.jcsr.2015.05.017.

[31] Heinisuo, M., Perttola, H. & Ronni, H. A step towards the 3D component method for modelling beam-to-column joints. *Steel Construction* **7**, 8–13 (2014). URL https://doi.org/10.1002/stco.201350001.

[32] Garifullin, M. *et al.* Effect of welding residual stresses on local behavior of rectangular hollow section joints. Part 1 – Development of numerical model. *Bauingenieur* **93**, 152–159 (2018).

[33] CEN. *Eurocode 3: Design of steel structures – Part 1-5: Plated structural elements (EN 1993-1-5:2006)* (Brussels, 2006).

[34] Packer, J., Puthli, R., van der Vegte, G. & Wardenier, J. Discussion on the paper "Experimental and numerical assessment of RHS T-joints subjected to brace and chord axial forces", by Nizer et al., Steel Construction 9 (2016), No. 4, pages 315–322. *Steel Construction* **10**, 89–90 (2017). URL https://doi.org/10.1002/stco.201770109.

[35] Garifullin, M., Bronzova, M., Heinisuo, M., Mela, K. & Pajunen, S. Cold-formed RHS T joints with initial geometrical imperfections. *Magazine of Civil Engineering* **4**, 81–94 (2018). URL https://doi.org/10.18720/MCE.80.8.

[36] Garifullin, M. *et al.* Effect of welding residual stresses on local behavior of rectangular hollow section joints. Part 2 – Parametric studies. *Bauingenieur* **93**, 207–213 (2018).

[37] Feldmann, M. *et al. Rules on high strength steel* (Publications Office of the European Union, Luxembourg, 2016). URL https://doi.org/10.2777/908095.

[38] Belytschko, T., Liu, W. K., Moran, B. & Elkhodary, K. I. *Nonlinear finite elements for continua and structures* (John Wiley & Sons, Chichester, United Kingdom, 2014), 2 edn.

[39] Bathe, K.-J. *Finite element procedures* (Klaus-Jurgen Bathe, Watertown, MA, United States of America, 2006), 2 edn.

[40] Havula, J., Garifullin, M., Heinisuo, M., Mela, K. & Pajunen, S. Moment-rotation behavior of welded tubular high strength steel T joint. *Engineering Structures* **172**, 523–537 (2018). URL https://doi.org/10.1016/j.engstruct.2018.06.029.

[41] Garifullin, M., Bronzova, M., Jokinen, T., Heinisuo, M. & Kovačič, B. Effect of fillet welds on initial rotational stiffness of welded tubular joints. *Procedia Engineering* **165**, 1643–1650 (2016). URL https://doi.org/10.1016/j.proeng.2016.11.905.

[42] Kanatani, H., Fujiwara, K., Tabuchi, M. & Kamba, T. *Bending tests on T-joints of RHS chord and RHS or H-shape branch* (CIDECT Programme 5AF, 1981).

[43] Zhao, X.-L. & Hancock, G. J. T-joints in rectangular hollow sections subject to combined actions. *Journal of Structural Engineering* **117**, 2258–2277 (1991). URL https://doi.org/10.1061/(ASCE)0733-9445(1991)117:8(2258).

Marsel Garifullin, Sami Pajunen, Kristo Mela, Markku Heinisuo
Tampere University of Technology
P.O.Box 600, FI-33101 Tampere, Finland
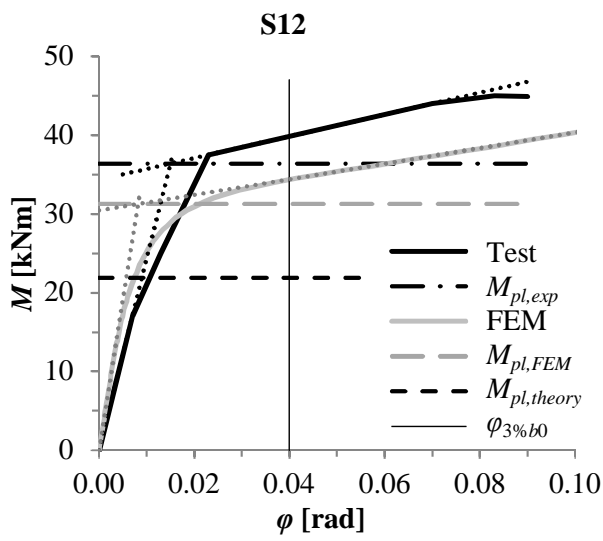marsel.garifullin@tut.fi, sami.pajunen@tut.fi, kristo.mela@tut.fi,
markku.heinisuo@tut.fi

Appendix 1. Load-displacement curves. HAMK tests

S420_S420_a6

S500_S420_a6

S500_S500_a6
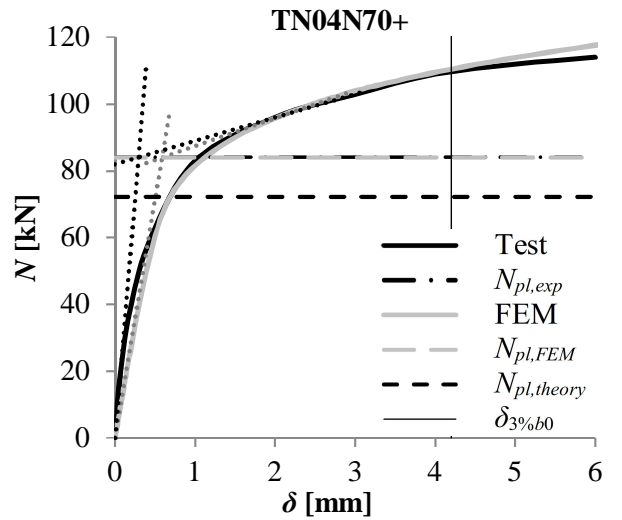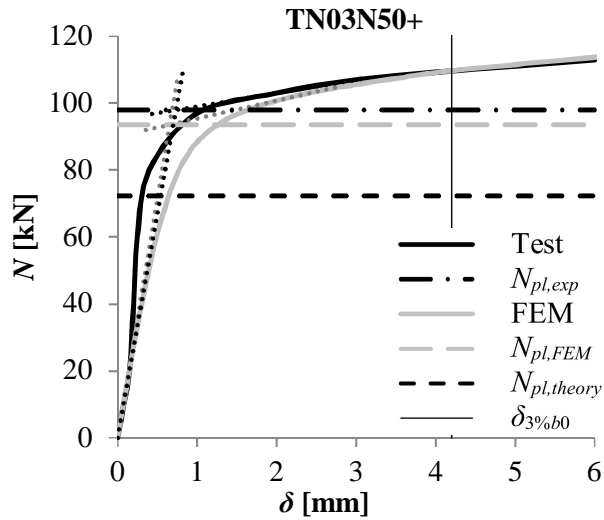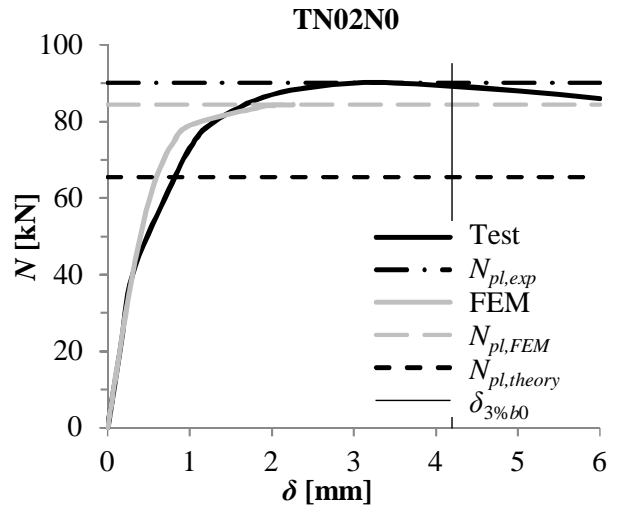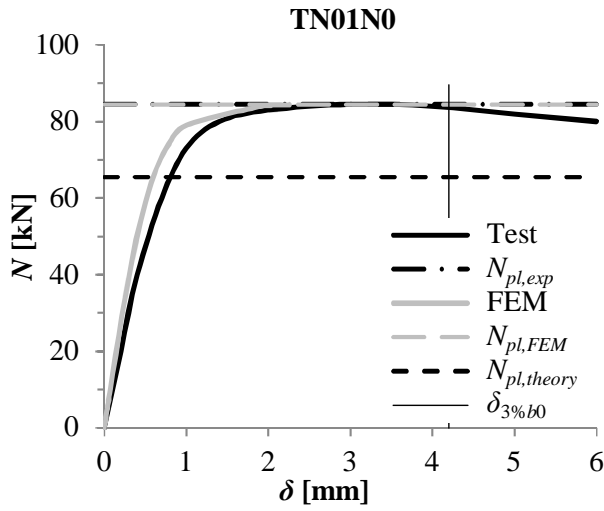

S700_S420_a6

S700_S500_a6

S700_S700_a6
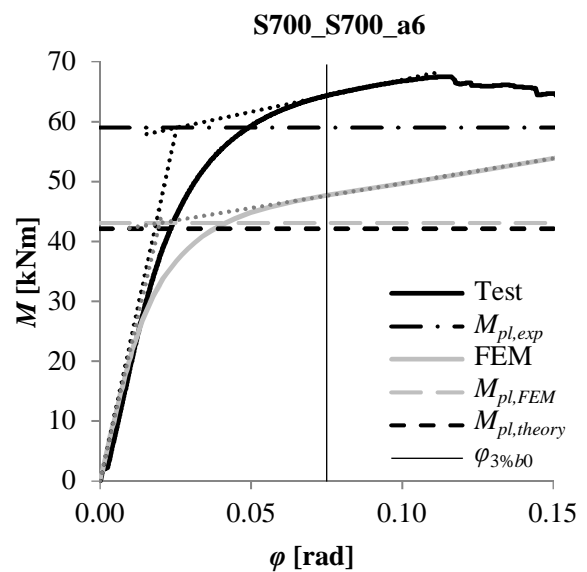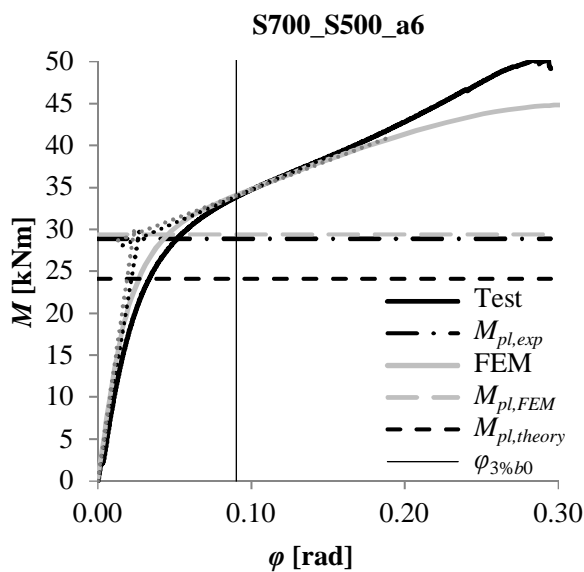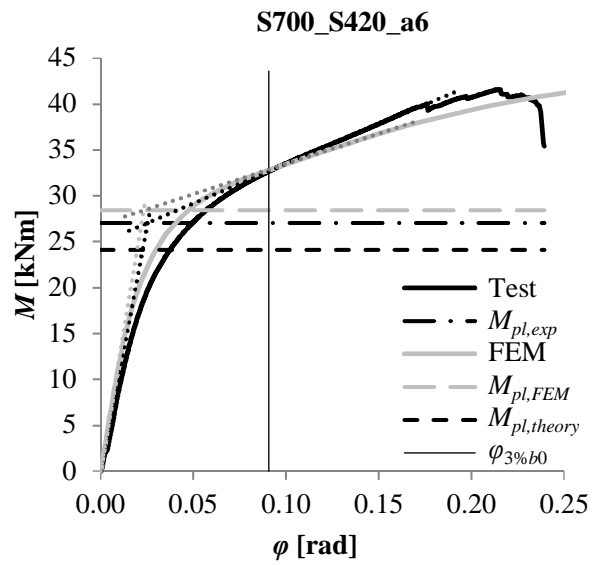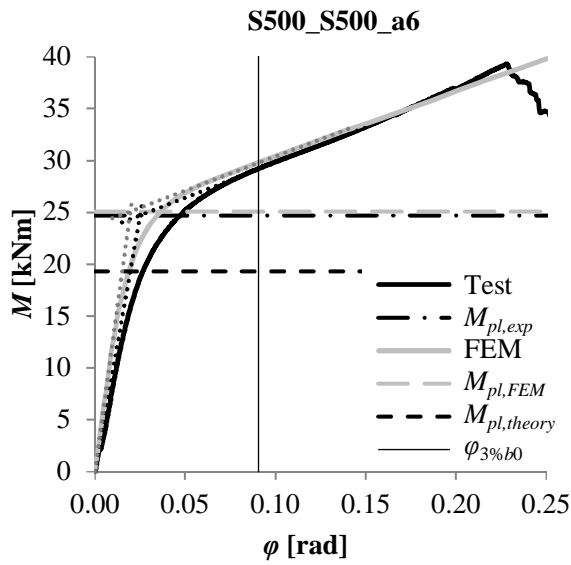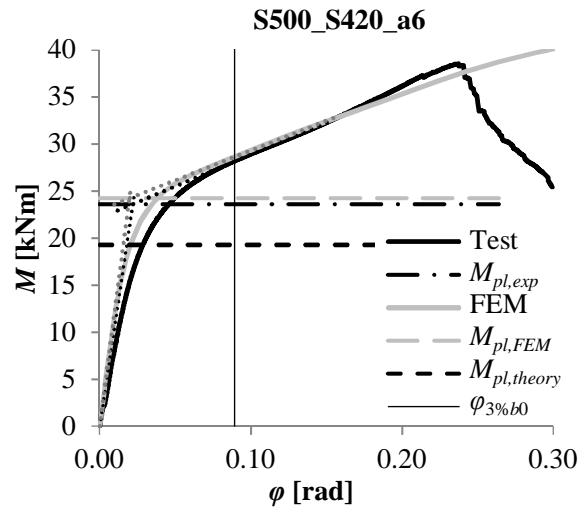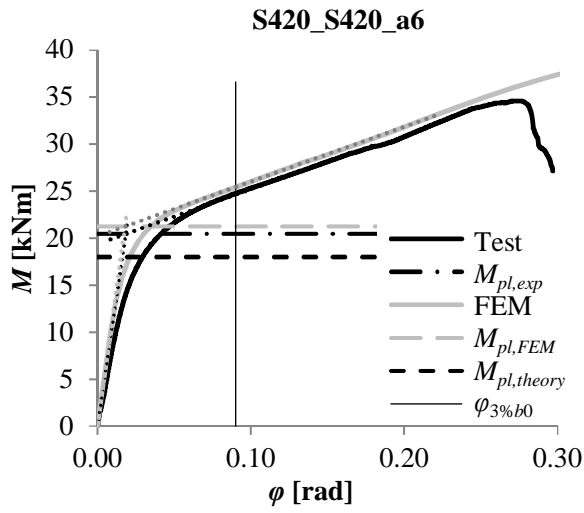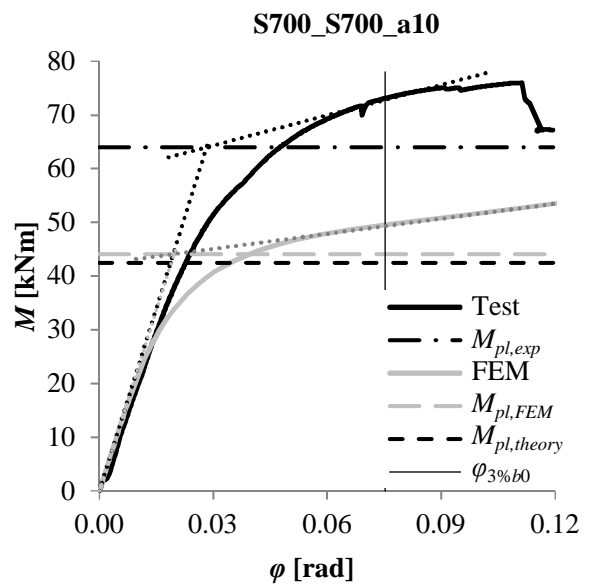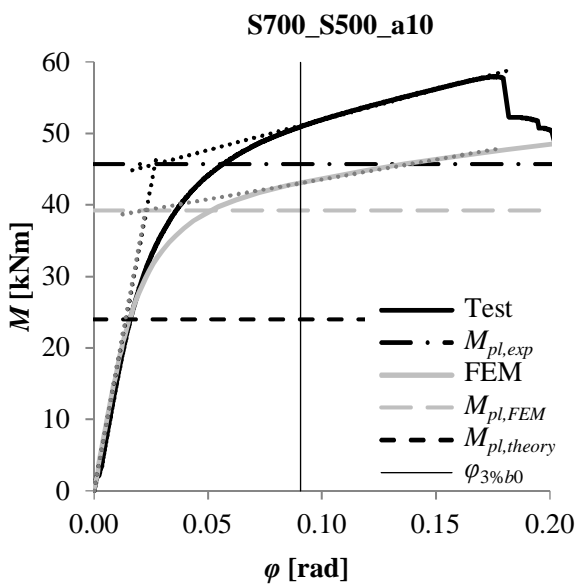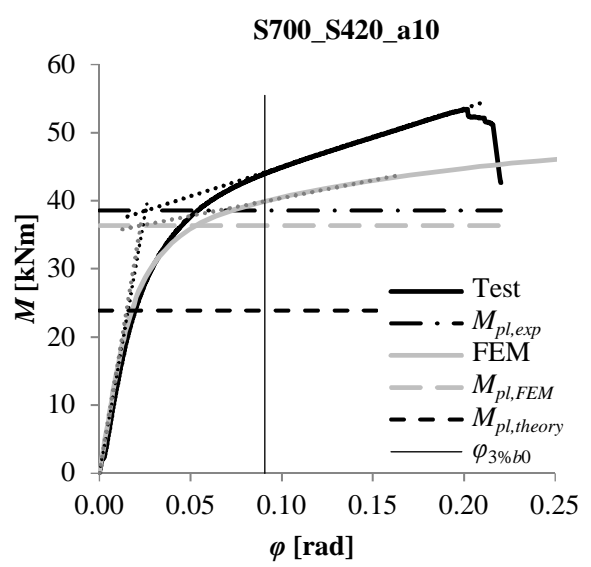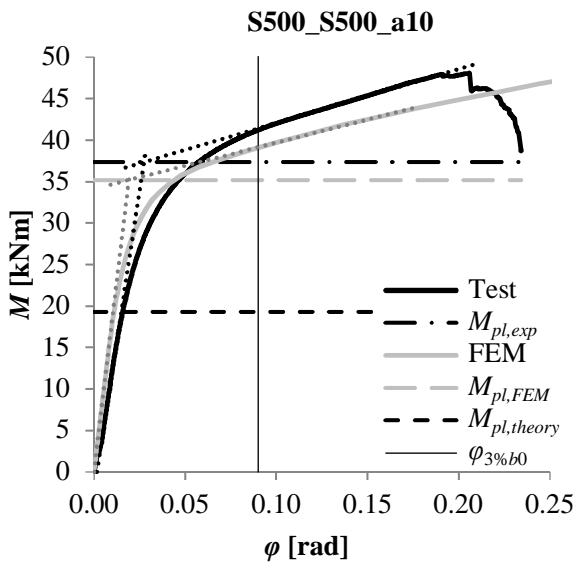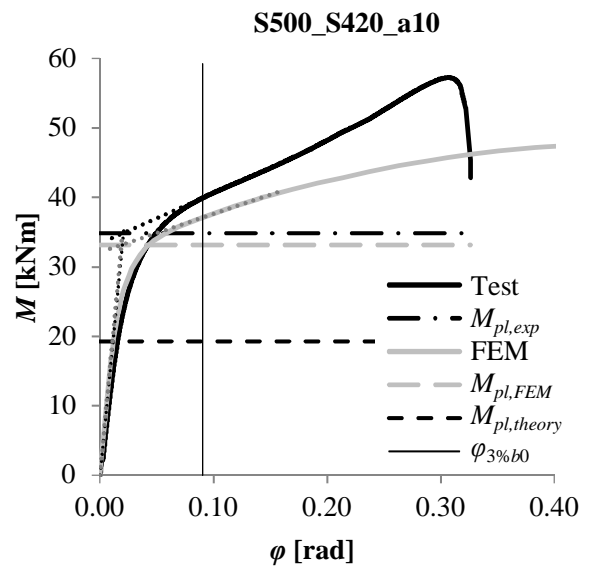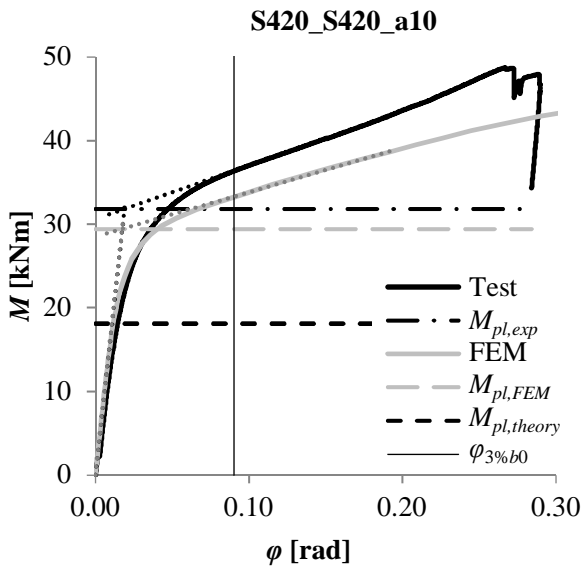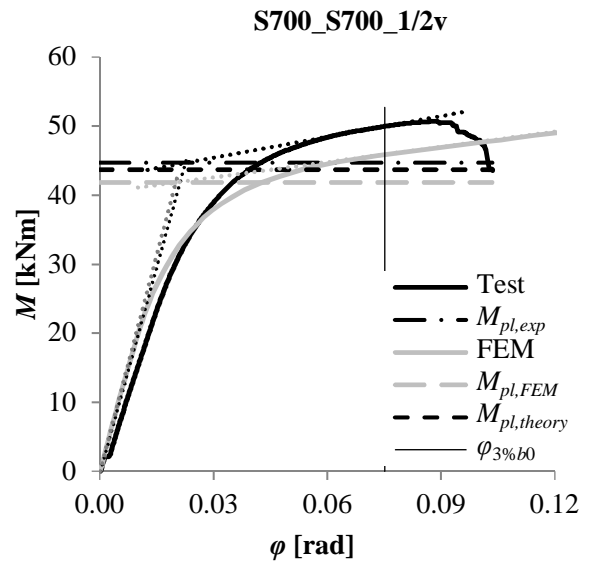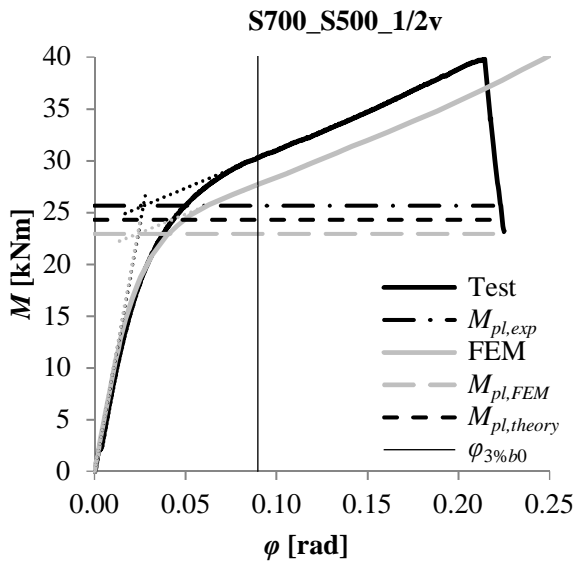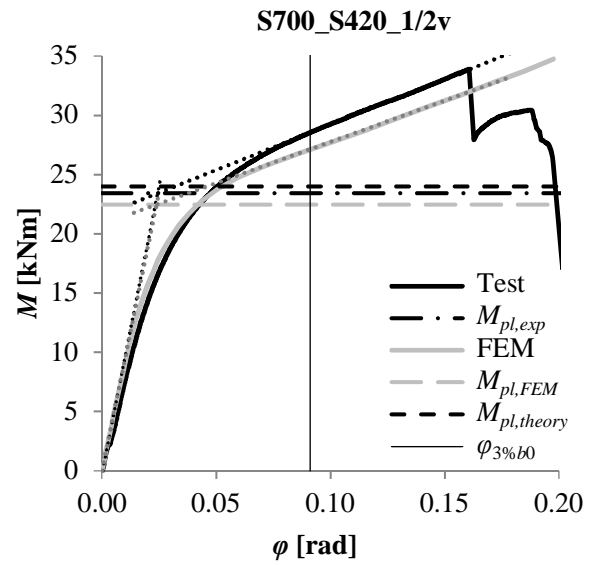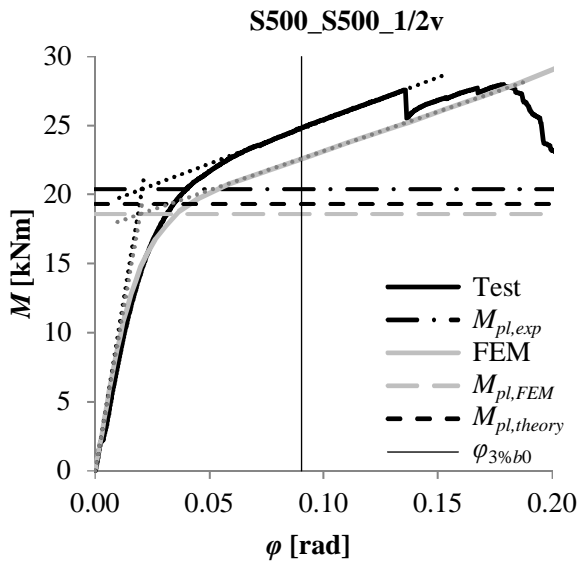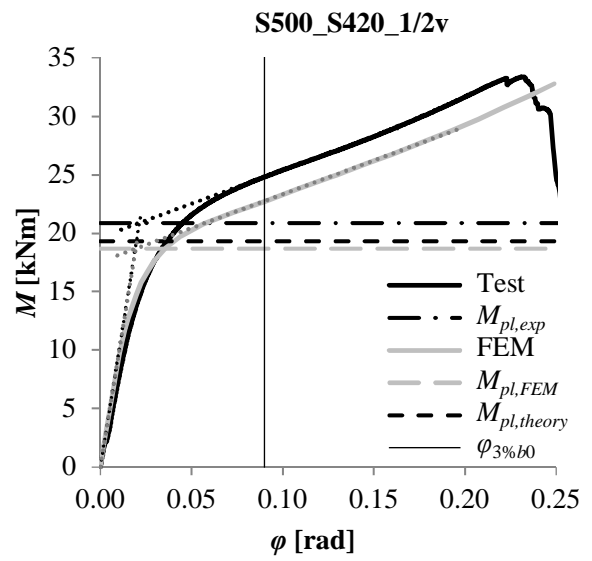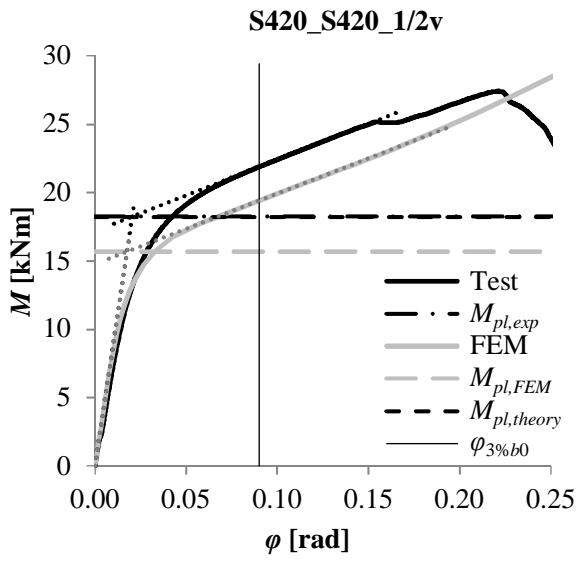
Appendix 2. Load-displacement curves. Tests of TH Karlsruhe and Kobe University
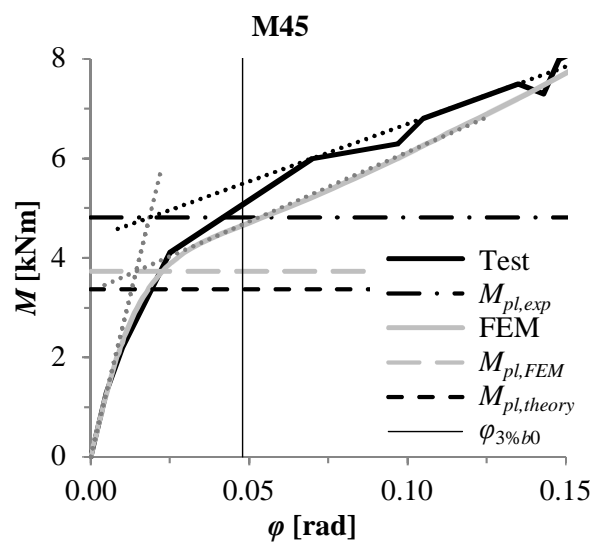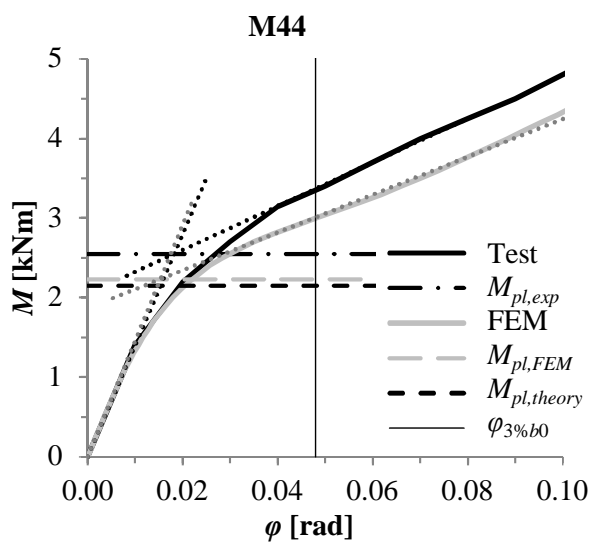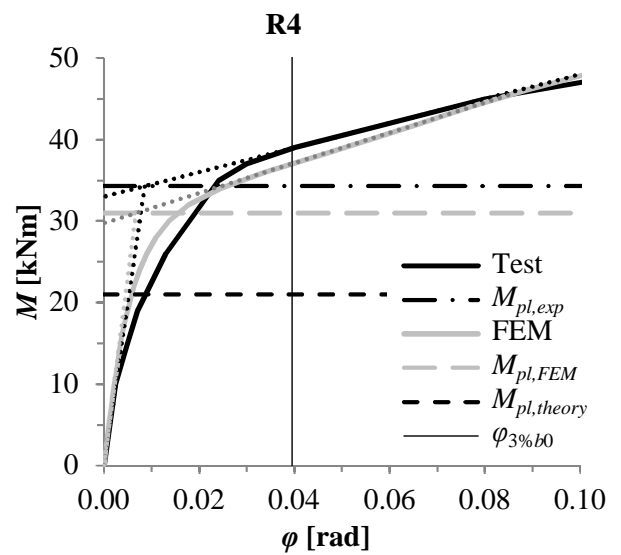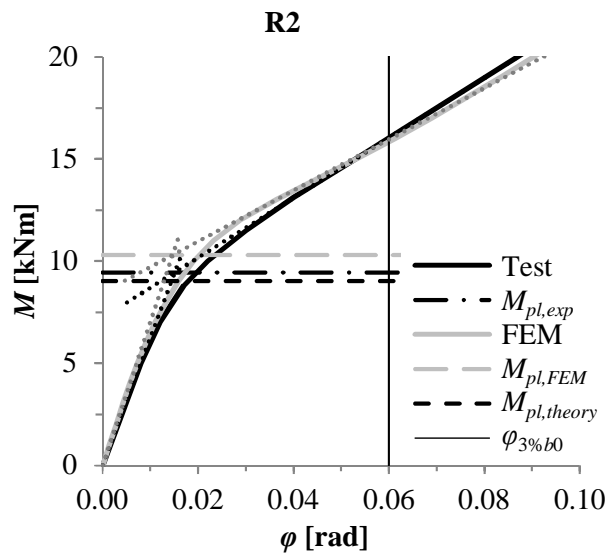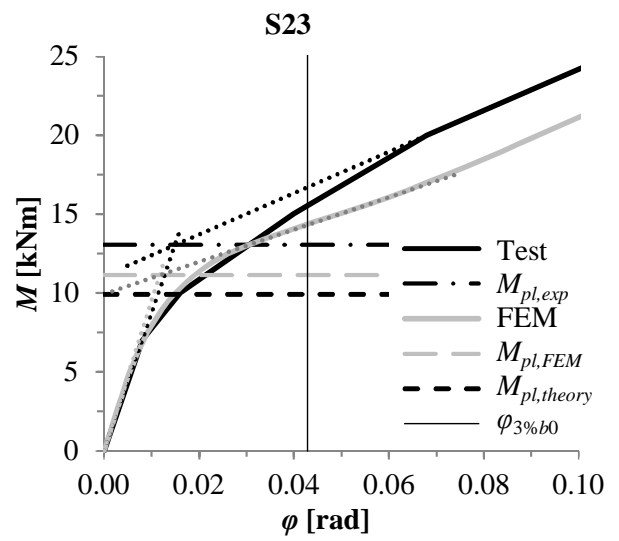
Appendix 3. Load-displacement curves. Tests of Nizer et al.

TN01N0

TN02N0

TN03N50+

TN04N70+

TN06N50-

TN05N70-
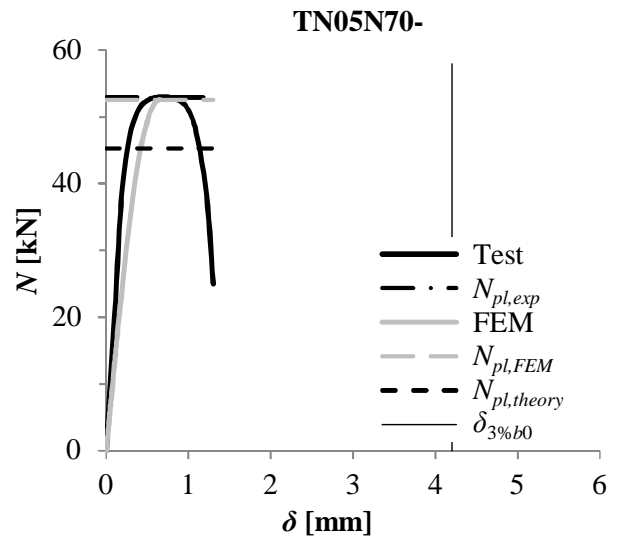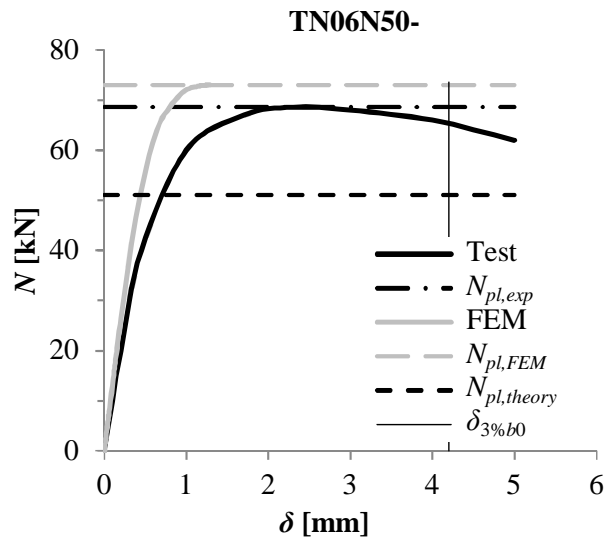
Appendix 4. Load-displacement curves. Tests of Zhao & Hancock

S1B1C11

S1B1C12

S1B1C23